Mixed transitions in the UV photodissociation of propargyl chloride revealed by slice imaging and mul- tireference ab initio calculations

Journal:	*Physical Chemistry Chemical Physics*
Manuscript ID	CP-ART-07-2018-004596.R1
Article Type:	Paper
Date Submitted by the Author:	06-Oct-2018
Complete List of Authors:	Foley, Casey; University of Missouri Columbia College of Arts and Science, Chemistry Joalland, Baptiste; University of Missouri Columbia College of Arts and Science, Chemistry Alavi, S. Tahereh; University of Missouri Columbia College of Arts and Science, Chemistry Suits, Arthur; University of Missouri Columbia College of Arts and Science, Chemistry

PCCP

ROYAL SOCIETY OF CHEMISTRY

ARTICLE TYPE

Cite this: DOI: 10.1039/xxxxxxxxxx

Mixed transitions in the UV photodissociation of propargyl chloride revealed by slice imaging and multireference ab initio calculations

Casey D. Foley, Baptiste Joalland, S. Tahereh Alavi, and Arthur G. Suits*

Received Date
Accepted Date

DOI: 10.1039/xxxxxxxxxx

www.rsc.org/journalname

Resonance-enhanced multiphoton ionization (REMPI) and DC slice imaging were used to detect photoproducts Cl ($^2P_{3/2}$), spin-orbit excited Cl* ($^2P_{1/2}$), and C_3H_3 in the photodissociation of propargyl chloride at 212 and 236 nm. Cl and Cl* translational energy distributions peak at high recoil energy, suggesting impulsive energy release in the C-Cl coordinate. Near 236 nm, photofragment angular distributions show rapidly changing anisotropy across the main peak for both Cl and Cl*, indicating excitations arising from in-plane or out-of-plane π systems. At 212 nm, the distribution is broader and isotropic for both Cl products. Ionization of C_3H_3 at 212 nm via 1+1 REMPI provides additional insight into these processes. A portion of the $C_3H_3^+$ distribution is momentum-matched to the Cl, but in addition, there is a component assigned to cyclic $C_3H_3^+$ formed from dissociative ionization of propargyl chloride. Multireference ab initio calculations show that excitations to three triplet states contribute at the long wavelength region, while predissociation from the first excited singlet state plays a role at the shorter wavelength.

1 Introduction

Photodissociation dynamics of alkyl halides continue to garner interest after decades of research.[1–8] Extensive experimental evidence of the photodissociation of methyl halides has revealed that dissociation via the first allowed electronic transition occurs directly from the nσ* state.[9–12] Though the primary dissociation process in methyl halides is C-X bond fission, HX elimination has been suggested as a channel for CH_3I[13] and was later reported in the photodissociation of CH_3Cl following excitation via the second absorption band.[14] Larger alkyl halides have more complex dissociation dynamics[2,8,15,16] and for π-bonded systems, there is an alternative set of possibilities due to the presence of multiple chromophores and excited states.[17,18] Decreasing the degree of saturation, as in vinyl chloride, nearly removes the contribution from nσ* and $\pi\sigma$* to the predominantly $\pi\pi$* excited state prior to C-Cl bond breaking from the excited state.[19] Allyl chloride also has multiple dissociation pathways with at least two HCl elimination channels and two mechanisms of liberating Cl.[20] For triple-bonded molecules such as propargyl chloride with two π systems, one coplanar with the carbon-halogen backbone, one perpendicular to it, interesting effects on the electronic structure and dissociation dynamics can be expected.

The first strong absorption in propargyl chloride has a maximum at 185 nm, so this transition is readily accessed at 193 nm where it has been studied in some detail. Both Cl and HCl products have been detected.[21–23] In 1984 Kawasaki and coworkers used photofragment translational spectroscopy to study the photodissociation of a range of halogenated hydrocarbons, including propargyl chloride. In that system they found m/z=35 (Cl^+) sharply peaked at high translational energies, while m/z=36 showed both low and high translational energy peaks. The high translational energy peak was attributed to momentum-matched $C_3H_3^+$ while the low energy portion was attributed to the HCl product. Overall, the fast fragments were attributed to fragmentation directly from a repulsive nσ* state, while the slow HCl was considered to be the result of intersystem crossing to a triplet state from the initially prepared $\pi\pi$* state. No product branching was reported because it was not possible to isolate the HCl^+ from the C_3^+ arising from C_3H_3 cracking upon electron impact ionization.

In 1996, Butler and coworkers used emission spectroscopy and configuration interaction-singles (CIS) ab initio calculations to investigate the contributions of various electronic configurations to the nominal $\pi\pi$* excited state in unsaturated hydrocarbon chlorides.[19] Vinyl chloride and cis-allyl chloride showed emission features analogous to ethylene, dominated by C=C stretch suggesting the clear $\pi\pi$* nature of the excitation. In propargyl chloride, both the C-Cl stretch and C=C stretch were prominent in the emission spectra, indicating that the molecule must initially be in an excited state with a high degree of σ* character. Ab initio calculations clearly supported these results, with vinyl chlo-

*Department of Chemistry, University of Missouri, 601 S. College Ave., Columbia, MO, USA 65211. Tel: 573-882-2976; *E-mail: suitsa@missouri.edu*

ride and cis-allyl chloride showing fairly simple π^* excited state character, while for propargyl chloride the transition was best described as excitation from the in-plane π orbital to a mixture of π^* and σ^*, with the latter dominant.

Soon after, Lee and Lin performed a photofragment translational spectroscopy study at 193 nm in which they observed a slow component in the m/z=35 product, which they assigned exclusively to fragmentation of HCl on ionization, leading to inferred Cl:HCl branching of 1:0.19.[22] Harper et al. later found that the Cl+/HCl+ fraction produced from electron impact ionization is 0.3, considerably lower than the 0.72 value estimated by Lee and Lin.[24] Furthermore, in 2003 Neumark and coworkers detected slow C_3H_3 fragments from propargyl chloride in photofragment translational spectroscopy experiments[25] using tunable VUV photoionization. Butler later observed the same,[23] likely due to improved signal to noise ratio. Butler, Pratt, and coworkers sought to resolve the HCl elimination and Cl product channel branching using velocity map imaging and resonance-enhanced multiphoton ionization (REMPI).[23] Using state-specific detection, they were also able to determine the relative contributions of ground state Cl ($^2P_{3/2}$) and spin-orbit excited Cl* ($^2P_{1/2}$) product channels. Approximately 95% of the Cl products were at high translational energy, in equal fractions of Cl and Cl*. Fragments at relatively low translational energy were only seen in the ground spin-orbit state, similar to what was previously observed in Cl photofragments of allyl chloride.[18]

Butler and coworkers also employed imaging with VUV (9.67 eV) photoionization of the C_3H_3 product, and found a good match between the Cl and C_3H_3 data with a slow component (5% in each). A clear assignment of the slow Cl channel was not possible, but two explanations were considered: either dissociation from a lower-lying electronic state of propargyl chloride, or formation of electronically excited propargyl radicals. HCl elimination was also detected using electron impact ionization and estimated to be between 10% and 30% branching for propargyl chloride dissocation at 193 nm. None of the several C_3H_2 isomers first produced as a cofragment of HCl were identified.

In a related study around the same time, Fan and Pratt examined propargyl bromide dissociation at 193nm with imaging detection of Br and Br* and tunable VUV ionization of C_3H_3. All distributions were bimodal, with a strong peak around 10 kcal/mol and a weak peak around 35 kcal/mol. The C_3H_3 data could be matched well assuming a 0.3 Br + 0.7 Br* branching. Tunable VUV from 8.97 to 9.86 eV was used to detect C_3H_3 both from C_3H_3Br and C_3H_3Cl, but no clear variation was seen in the spectra. A later investigation of C-Br bond fission dynamics with dissociation at 234 nm observed high and low kinetic energy components corresponding to two dissociation channels.[26] The high kinetic energy channel was explained as direct dissociation from a singlet nσ^* state while the low kinetic energy channel was attributed to internal conversion to a lower lying triplet state. A highly mixed excited state character based on Br angular distributions was also reported.

Propargyl chloride photodissociation studies have so far primarily sought to determine the branching in dissociation channels that originate from the strong absorption near 193 nm. Here, we present an imaging investigation of propargyl chloride dissociation at longer wavelengths, with state-specific detection using REMPI probe of Cl and Cl* and 1+1 ionization of C_3H_3. The experimental data is interpreted with the aid of multireference calculations to characterize the nature of the electronic excitations.

2 Methods

2.1 DC Slice Imaging

The experimental method and apparatus were previously reported,[27] but a brief description of relevant information is included here. The apparatus consists of source and detection chambers separated by an aluminum plate on which a skimmer is mounted. Each chamber is pumped by a separate turbomolecular pump. A molecular beam of propargyl chloride, C_3H_3Cl, was introduced into the source chamber via a pulsed solenoid valve (Parker-General) and subsequently skimmed and supersonically expanded. 7% C_3H_3Cl was generated by passing helium through C_3H_3Cl in a bubbler at 0°C. UV radiation at wavelengths near 212 and 236 nm was focused onto the molecular beam with a 30 cm focal length fused silica lens. These wavelengths were chosen for specific Cl and Cl* REMPI transitions: For Cl and Cl* the experiments are all "one-color" dissociation and probe. For Cl detection the transitions were $^2D^\circ_{3/2} \leftarrow ^2P^\circ_{3/2}$ (84988.48 cm^{-1}) and $^2P^\circ_{3/2} \leftarrow ^2P^\circ_{3/2}$ (94314.21 cm^{-1}), while for Cl*, the transitions were $^2P^\circ_{3/2} \leftarrow ^2P^\circ_{1/2}$ (84560.08 cm^{-1}) and $^2P^\circ_{3/2} \leftarrow ^2P^\circ_{1/2}$ (93431.85 cm^{-1}).[28,29] In each case, the wavelength was scanned repeatedly across the Doppler profile while recording the images. For C_3H_3 detection, the light was detuned slightly from the Cl or Cl* transition. All UV light was polarized vertically, parallel to the plane of the detector. The resulting ions were accelerated by an ion optics assembly through a time-of-flight tube toward a pulsed 75 mm microchannel plate detector (BOS-75-OPT01, Beam Imaging Solutions) coupled to a P-47 phosphor screen for DC slice ion imaging. Images were captured using a USB CCD camera and in-house data acquisition software NuACQ. Time-of-flight information was obtained with a photomultiplier tube monitoring the phosphor screen. The experiment was performed at 10 Hz. Image reconstruction and data extraction were done using our finite slice analysis method, FinA.[30,31] This analysis has been shown to yield accurate angular distributions, giving β values within 0.02 typically. Uncertainties in the energy-dependent β values are dominated by statistics as may be inferred from the noise in the plots.

2.2 Quantum Chemistry Calculations

The global minima on both singlet and triplet ground state potential energy surfaces of C_3H_3Cl were optimized at the CCSD(T) level with the cc-pVTZ basis for H and C[32] and aug-cc-pVTZ for Cl[33,34] (designated as aug(Cl)-cc-pVTZ), followed by frequency calculations in the harmonic approximation. The singlet-triplet separation was thus determined including correction for zero-point energy (ZPE). Single-point calculations at the CCSD(T) optimized geometry of the singlet ground state $^1A'$, which belongs to the C_s group, were performed with various multireference methods to assess the energy levels in the Franck-Condon (FC) region.

Complete active space self-consistent field (CASSCF)[35,36] calculations were used with the wave function state-averaged over 12 states ($3 \times {}^1A'$, $3 \times {}^1A''$, $3 \times {}^3A'$, $3 \times {}^3A''$, "SA12-CASSCF"). Several active spaces were tested, i.e. 14 electrons in 13 orbitals (8 a' and 5 a''), 14 electrons in 11 orbitals (7 a' and 4 a''), 10 electrons in 11 orbitals (7 a' and 4 a''), and 10 electrons in 9 orbitals (6 a' and 3 a''). For both 14/11 and 10/9 active spaces, the CASSCF wave functions were used to perform XMS-CASPT2 calculations (multi-state complete active space, second order perturbation theory) in order to treat dynamical electronic correlation (imaginary level shift of 0.4 a.u.),[37] while the CASSCF(10/9) wave function was also used for MRCI-F12 calculations, which provides here the most accurate evaluation of the energy levels after Davidson's correction.[38] Additionally, two types of CASSCF scans were performed. First, CASSCF(10/9) single point calculations along the $\mathbf{q}_{14}$ vibrational mode, an antisymmetric CCC bend located at 301 cm^{-1} at the CCSD(T) level (and likely to be significantly populated), were carried out in order to evaluate which states might exhibit vibronic couplings due to the occurrence of double-wells along this coordinate, as pointed out by Eisfeld in the case of propargyl radical. The wave function was state-averaged over the 6 first singlet states. Second, CASSCF(10/11) single point calculations were performed along the C-Cl coordinate, with geometry relaxed on the singlet ground state at the MP2 level of theory.[40] In this case the wave function was state averaged over the six singlets and six triplets states mentioned above, which merge in two mixed asymptotes as $R \to \infty$, *i.e.* C_3H_3 + Cl and C_3H_3* + Cl. For both CASSCF scans, the cc-pVTZ basis set was used for H, C, and Cl. All calculations were performed with MOLPRO.[41]

3 Results

We first present imaging results for UV dissociation of propargyl chloride near 236 nm. Figure 1 shows DC slice images obtained for detection of ground state Cl atom at 235.326 nm and for spin-orbit excited Cl* at 236.518 nm. The Cl image in Fig. 1A exhibits two components: a broad inner ring and a sharp outer ring. Both regions show recoil preferentially oriented along the laser polarization direction. The Cl* image in Fig. 1B shows a single ring, which is wider on the sides than on the poles. This unusual feature arises from an inner perpendicular distribution overlapping with an outer nearly-isotropic distribution. Figs. 2A and B give the total translational energy distributions $P(E_T)$ obtained from the images in Figs. 1A and B, respectively. Superimposed on the translational energy distributions in Fig. 2A and B are the associated angular distributions given as a function of translational energy. The angular distributions are obtained by fitting the image at each radius to the well-known expression

$$I(\theta) \propto 1 + \beta(P_2(\cos\theta)) \quad (1)$$

where P_2 is the second Legendre polynomial, and β characterizes the photofragment angular distribution, ranging from -1 ("perpendicular") to +2 ("parallel") for the case of linear photolysis polarization.

We first examine the Cl* distributions, as they allow to understand the Cl distributions more clearly. The inner, perpendicular

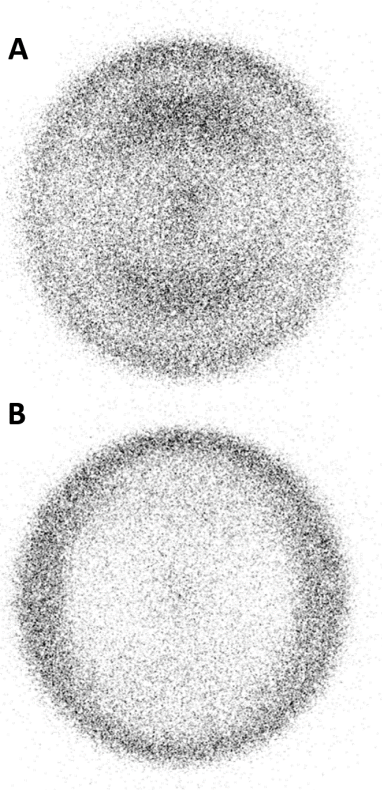

Fig. 1 DC slice images of Cl (A) and Cl* (B) from photodissociation of propargyl chloride near 236 nm. Laser polarization axis is vertical.

component of the Cl* translational energy distribution appears as a shoulder with a maximum around 20 kcal/mol, with the primary peak reaching a maximum around 26 kcal/mol. The corresponding β values reach a minimum of -0.5 near the peak of the inner shoulder, but then rise to slightly positive values. The ground state Cl translational energy distribution appears bimodal as we have noted above. The angular distributions of Cl and Cl* show clear similarities for the outer peak. Ignoring for the moment the distinct low energy peak around 10 kcal/mol, the main peak shows the same trend as Cl*, with a minimum in β around 20 kcal/mol that rises sharply to a substantially more parallel value, although for the Cl case all β values are positive. This suggests that the main peak is also composite, consisting of overlapping components peaking around 20 and 26 kcal/mol just as for Cl*. The additional lower energy peak is even more strongly parallel, with β values approaching +0.8.

Fig. 3 shows DC slice images for photodissociation near 212 nm. Fig. 3A is the sliced image for Cl, Fig. 3B is Cl*. and Fig. 3C is an image obtained at m/z=39, C_3H_3. We did not detect m/z=39 in the vicinity of the 236 nm excitation. The ground state Cl image shows a fast sharp ring that appears somewhat perpendicular, along with a weaker slow isotropic feature barely visible inside the fast sharp ring. The Cl* Image shows a bimodal distribution with features that appear to be largely isotropic. The C_3H_3 image shows two main components that are somewhat parallel: A fast outer ring that matches with the Cl and Cl* images

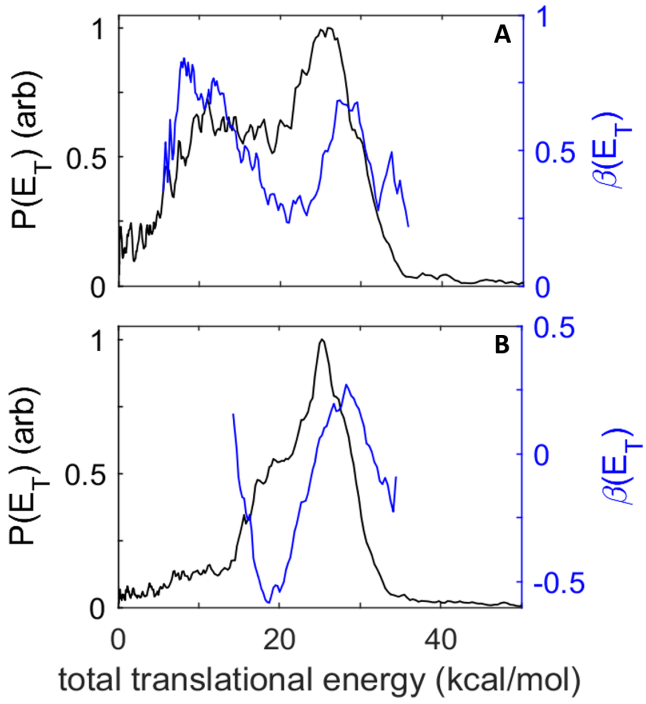

Fig. 2 Translational energy distributions (black) and anisotropy parameter β (blue) of Cl (A) and Cl* (B) from photodissociation of propargyl chloride near 236 nm.

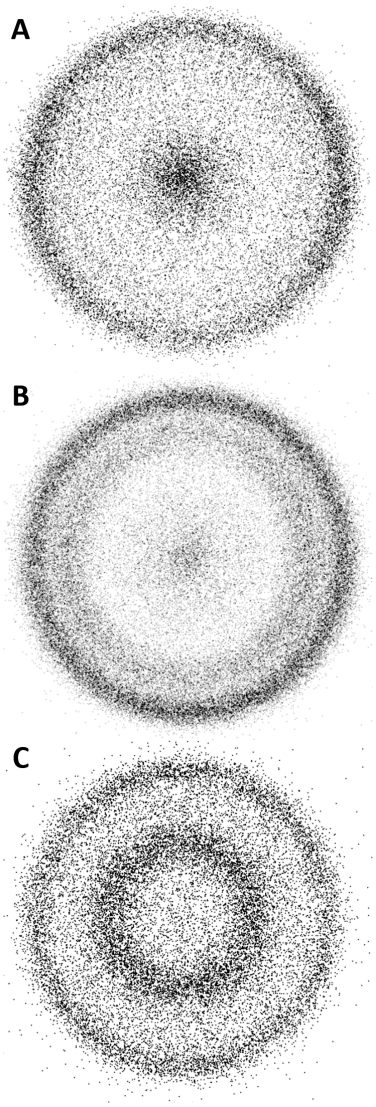

Fig. 3 DC slice images of Cl (A), Cl* (B), and C_3H_3 (C) from photodissociation of propargyl chloride near 212 nm. Laser polarization axis is vertical.

and a sharp inner ring that does not appear in the Cl atom images. The secondary inner ring that appears in the Cl* image does not appear clearly in the C_3H_3 images. The translational energy and energy-dependent angular distributions derived from the images in Fig. 3 are shown in Fig. 4. The Cl distribution shows the main fast peak around 32 kcal/mol, tapering to lower energy suggesting some evidence of a second component as in the Cl* image. That inner component shows a β near zero, but the main peak is consistently perpendicular ($\langle\beta\rangle$ =-0.3). The Cl* distribution has an analogous fast feature, along with a distinct component associated with the inner ring. The angular distribution overall is largely isotropic but varies from β=-0.2 to 0.2 across the two components. The C_3H_3 translational energy distributions can be seen to be a combination of a component momentum-matched to the Cl and Cl* and a distinct feature peaking around 10 kcal/mol mentioned above. The energy dependent β values range from near 0 to around 0.4.

Theoretical calculations of the propargyl radical absorption spectrum by Eisfeld indicate a strong $2^2B_1 \leftarrow 1^2B_1$ electronic absorption beginning around 335 nm, and a much weaker one, identified as $3^2B_1 \leftarrow 1^2B_1$, extending from 240 nm to 185 nm, with a vertical maximum near 206 nm.[39] We believe the fast outer ring in the C_3H_3 image in Fig. 3C results from 1+1 REMPI via this $3^2B_1 \leftarrow 1^2B_1$ transition. The relatively intense inner feature in the C_3H_3 that does not match the Cl data must have a different origin entirely. As discussed below, we can readily assign this feature to 2-photon dissociative ionization of propargyl chloride yielding the aromatic c-$C_3H_3^+$ ion with Cl, while the sharp cut-off on the low-energy side likely reflects secondary decomposition of the hot c-$C_3H_3^+$ ion.

4 Discussion

We first reproduce the absorption spectrum recorded by Fahr *et al.* for propargyl chloride (Fig. 5) to guide the following discussion.[42,43] Marked on the figure are the two wavelength regions examined here in addition to the well-studied 193 nm excimer line. For propargyl chloride, the first strong absorption appears at 185 nm, while for propargyl bromide this excitation is shifted to slightly longer wavelength.[42,43] In addition, for propargyl bromide there is a weak broad maximum around 230 nm that is up to two orders of magnitude weaker in the propargyl chloride spectrum, strongly suggesting a triplet excitation present in this vicinity. The results of our multireference calculations at the MRCI-F12/aug(Cl)-cc-pVTZ level, also shown in Fig. 5, confirm the presence of a series of low-lying triplet states, the first of which, $1^3A'$ (T_1) has a vertical excitation energy of 5.39 eV, which is very

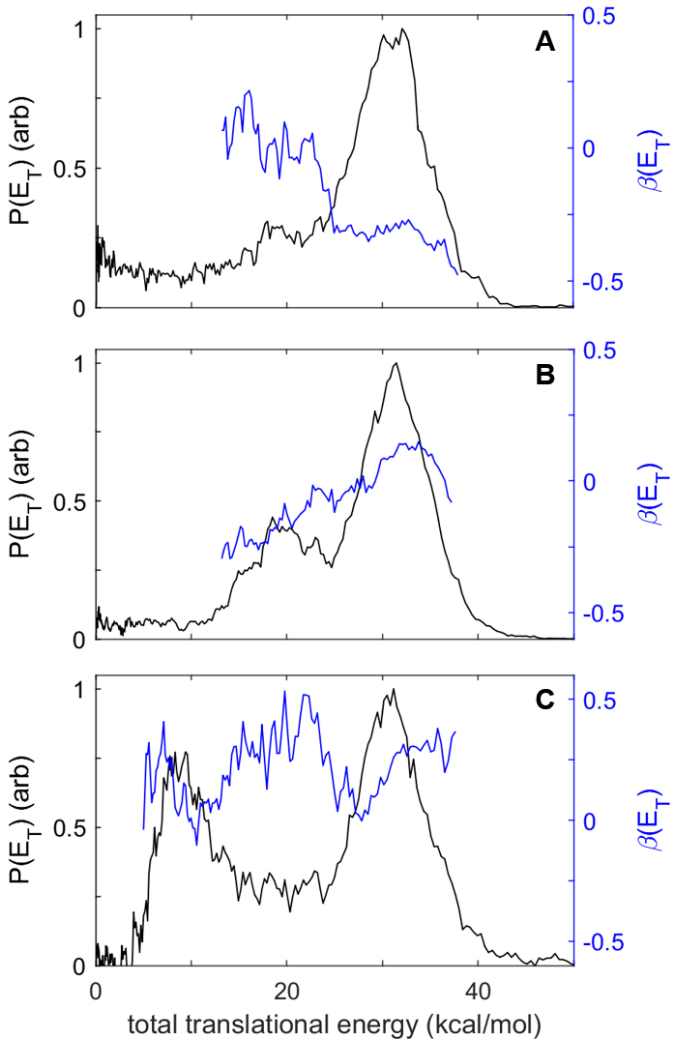

Fig. 4 Translational energy distributions (black) and anisotropy parameter β (blue) of Cl (A), Cl* (B), and C_3H_3 from photodissociation of propargyl chloride around 212 nm.

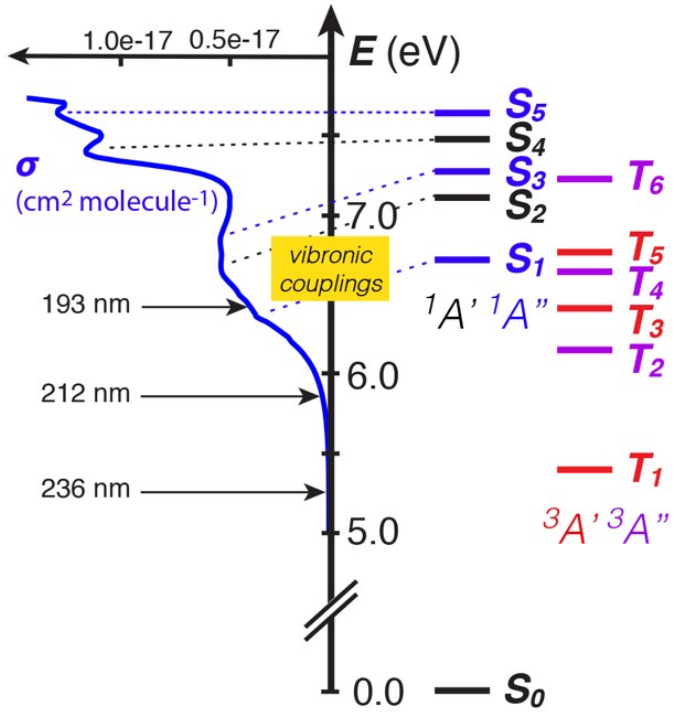

Fig. 5 Absorption spectrum of propargyl chloride (left, blue) at 295 K (adapted from Fahr *et al.*[42]) and excitation energies of the singlet and triplet states located below 8 eV ($3 \times {}^1A'$ (black), $3 \times {}^1A''$ (blue), $3 \times {}^3A'$ (red), $3 \times {}^3A''$ (purple)) calculated at the MRCI-F12/aug(Cl)-cc-pVTZ level. Laser excitation wavelengths are shown with black arrows and a tentative assignment of the features observed in the experimental spectrum with dashed lines. Note that strong vibronic couplings are expected for excitations to the S_1, S_2, S_3, and S_4 states due in part to the presence of double-wells along the low-frequency CCC bending coordinate (see Fig. S1 in ESI†).

near the photon energy at 236 nm. Following T_1 are a pair of states, $1\,^3A''$ and $2\,^3A'$ (T_2 and T_3) very close at 6.15 and 6.41 eV, respectively. There are additional triplets at higher energy, but for our purpose the next transition of importance is likely the first singlet excited state $1\,^1A''$ (S_1) at 6.71 eV. We note the vertical transitions to the lower singlet states appear at higher energy than the associated features in the spectrum. This is ascribed to vibronic coupling, likely involving the antisymmetric CCC bending mode (ν_{14}) along which S_1, S_2, S_3, and S_4 are found to exhibit double-wells (see Fig. S1 in ESI†)

In the following, we refer to the potential energy cuts given in Fig. 6. We first consider the inner component of the ground state Cl product at 236 nm, which peaks at 11 kcal/mol total translational energy and shows considerable anisotropy. There is no related contribution in the Cl* distribution, and as we move to shorter wavelength, this component disappears entirely. We assign this contribution to excitation to the T_1 state, which results in ground state products and does not cross another potential surface along the reaction coordinate. We then find the two nearly overlapping peaks that appear both in Cl and Cl* images and translational energy distributions. In this case, for Cl* the inner peak is strongly perpendicular, while the outer peak is predominantly parallel. In fact, the same trend is seen for the Cl data, but shifted to higher β values. This suggests excitations that branch to both products, with the perpendicular component branching more to Cl*. We can thus clearly associate the perpendicular contribution with the $1\,^3A''$ state, T_2, and the outer, parallel component with the $2\,^3A'$ state, T_3. According to the calculations, these are separated by only 0.26 eV in the FC region. A crossing of these surfaces is seen in Fig. 6, with the lower $1\,^3A''$ likely preferentially following a nonadiabatic path to the Cl* asymptote.

Around 212 nm, the striking aspect of the data is that the angular distributions are now nearly isotropic except for the main peak for the Cl case. Moreover, for the Cl*, two well-separated components appear, peaking at 20 and 32 kcal/mol. We assign these to predissociation, likely by the same triplet states, following excitation to the bound S_1 state. Considering the $C_3H_3^+$ data,

Table 1 Summary of theoretical calculations. Structures of the ^{1}A' and ^{3}A minima optimized at the CCSD(T) level, along with singlet-triplet separation energy ΔE including ZPE correction. Excitation energies from the ground state singlet to the first 5 singlet and 6 triplet states calculated with various active spaces and multireference methods at the optimized CCSD(T) singlet ground state geometry. Oscillator strengths of the singlet-singlet transitions estimated from SA6-CASSCF(10/9) transition dipole moments and SA12-MRCI-F12+Q energies. All calculations were done with the aug(Cl)-cc-pVTZ basis set. Energies are expressed in eV.

CCSD(T)	S_0 **geometry (^{1}A')**	ΔE (eV)	T_1 **geometry (^{3}A)**
	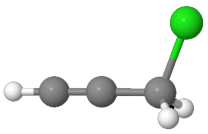 *side view*		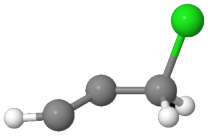 *side view*
		3.97	
	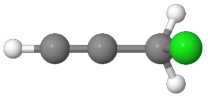 *top view*		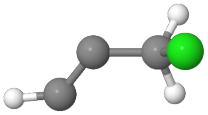 *top view*

	Vertical excitation energies (eV)										
	$1\,^1A'$ S_2	$2\,^1A'$ S_4	$1\,^1A''$ S_1	$2\,^1A''$ S_3	$3\,^1A''$ S_5	$1\,^3A'$ T_1	$2\,^3A'$ T_3	$3\,^3A'$ T_5	$1\,^3A''$ T_2	$2\,^3A''$ T_4	$3\,^3A''$ T_6
SA12-CASSCF											
(14/13)	7.81	8.17	7.32	7.89	8.16	5.57	6.55	7.26	6.50	7.07	7.56
(14/11)	7.68	8.08	7.21	7.82	8.22	5.51	6.54	7.13	6.45	7.01	7.54
(10/11)	7.96	8.61	7.39	8.14	8.43	5.57	6.56	7.70	6.54	7.42	7.58
(10/9)	7.89	8.26	7.37	7.97	8.17	5.57	6.55	7.31	6.52	7.08	7.58
XMS-SA12-CASPT2											
(14/11)	6.74	7.17	6.33	6.86	7.39	5.11	6.04	6.33	5.83	6.25	6.92
(10/9)	6.75	7.22	6.41	6.80	7.37	5.13	6.04	6.31	5.89	6.20	6.92
SA12-MRCI-F12+Q											
(10/9)	7.10	7.47	6.71	7.26	7.64	5.39	6.41	6.76	6.15	6.63	7.24
	Oscillator strengths										
CASSCF/MRCI-F12+Q	0.013	0.000	0.001	0.003	0.004						

the outer region agrees well with the Cl/Cl* data, and we ascribe this signal to ionization of the propargyl radical photoproduct by 1+1 ionization through the $3\,^2B_2 \leftarrow 1\,^2B_2$ transition, which Eisfeld finds has a maximum around 220 nm.[39] It is not clear, however, whether there is important vibrational selectivity in this REMPI process. The good agreement between the Cl/Cl* and $C_3H_3^+$ signals on the shape of the outer peak suggests there is no strong selectivity over the levels produced there. The bimodal distribution observed in the Cl* data is much weaker in the Cl distribution and although not readily apparent in the image, it shows up in the integrated distribution. The anisotropy seen in the Cl image is not present in the Cl* nor in the C_3H_3+, suggesting this is the result of angular momentum alignment that modulates the sensitivity in these one-color experiments. Indeed, in separate two-color experiments to be reported elsewhere we find evidence for alignment in the Cl atom following dissociation in the deep UV, but not at 230 nm or longer. The puzzling aspect of reconciling the Cl/Cl* data and the C_3H_3 result is that the latter angular distributions appear overall somewhat parallel and do not match any combination of the Cl and Cl* distributions. Given our lack of a detailed understanding of the C_3H_3 ionization process and the noise in the data, we place less confidence in the C_3H_3 angular distributions.

The intense peak at 10 kcal/mol in the $C_3H_3^+$ has no corresponding contribution in the Cl signals, therefore it does not arise from ionization of a C_3H_3 photoproduct. Instead, it results from 2-photon dissociative ionization of propargyl chloride via the S_1 state. The total two-photon energy here is 11.58 eV. The appearance energy of $C_3H_3^+$ from propargyl chloride has been reported as 11.02 eV, and the product ion in this case has been identified as the cyclopropenium cation.[44] Given the 0 K heats of formation of *c*-$C_3H_3^+$ (256.9 kcal/mol), Cl (28.6 kcal/mol) and C_3H_3Cl (44.6 kcal/mol),[45,46] we find the available energy for this channel to be 1.18 eV or 27 kcal/mol. The barrier for Cl elimination to form *c*-$C_3H_3^+$ is indicated by the onset of the peak at 8 kcal/mol, in good agreement with the earlier estimate of 0.32 eV.[44] An interesting aspect of the $2\,^3A''$, T_4 state is the potential well correlated with

Table 2 Energy partitioning of the Cl/Cl* photofragments at indicated nominal wavelength. Precise excitation energies are given in Methods. The 0 K dissociation energy, 68.6 kcal/mol, is obtained from reference 46. E_{tot} and E_{avl} stand for excitation energy and available energy after dissociation on the ground state, respectively, E_T for the translational energy of each Cl/Cl* peak, E_{int}, E_{rot}, and E_{vib} for the internal, rotational, and vibrational energies of C_3H_3 according to the impulsive model (see text for details). f_{vib} and f_T are the fractions of available energy appearing in C_3H_3 vibrational and total translational energies, respectively. Energies are expressed in kcal/mol.

Cl									Cl*								
λ (nm)	E_{tot}	E_{avl}	E_T	E_{int}	E_{rot}	E_{vib}	f_{vib}	f_T	λ (nm)	E_{tot}	E_{avl}	E_T	E_{int}	E_{rot}	E_{vib}	f_{vib}	f_T
235.3	123.2	54.6	27	27.6	18.4	9.3	0.17	0.49	236.5	122.6	51.5	27	24.5	18.4	6.1	0.12	0.52
235.3	123.2	54.6	19	35.6	12.9	22.7	0.42	0.35	236.5	122.6	51.5	19	32.5	12.9	19.5	0.38	0.37
235.3	123.2	54.6	11	43.6	7.5	36.2	0.66	0.20									
212.1	136.8	68.2	31	37.2	21.1	16.1	0.24	0.45	214.1	135.5	64.3	31	33.3	21.1	12.2	0.19	0.48
212.1	136.8	68.2	19	49.2	12.9	36.2	0.53	0.28	214.1	135.5	63.9	20	44.3	13.6	30.7	0.48	0.31

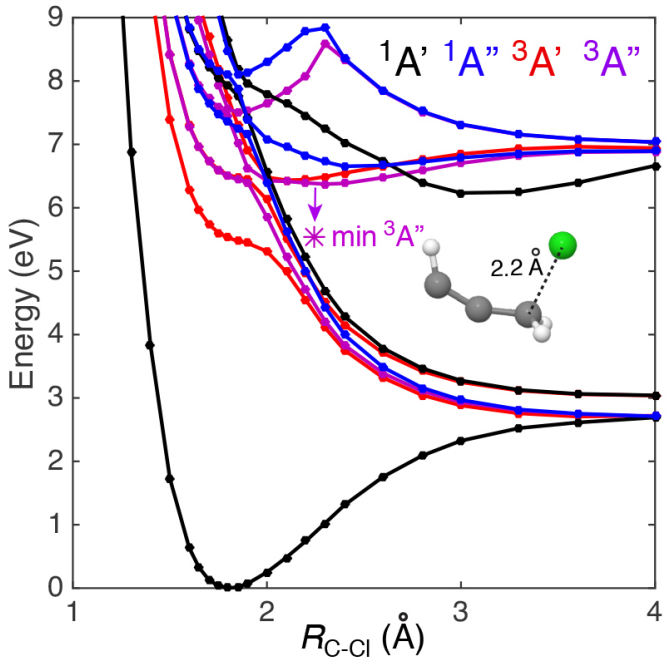

Fig. 6 Potential energy cuts along the R_{C-Cl} coordinate leading to the C_3H_3 + Cl and C_3H_3* + Cl asymptotes. The level of theory is SA12-CASSCF(10/11)/cc-pVTZ and the geometry is relaxed on the ground state by optimization at the MP2/cc-pVTZ level. The color code for state symmetry and multiplicity is the same as in Fig. 5. The molecular structure corresponds to a minimum on the **2** $^3A''$ state, which correlates to the C_3H_3* + Cl asymptote and could play a role as an intermediate before the dissociation occurs towards the ground state.

the C_3H_3* + Cl asymptote. The molecular structure of this minimum is displayed in Fig. 6 and we note this as a possible long-lived intermediate before dissociation occurs towards the ground state products.

These results may be contrasted with the 193 nm dissociation studied by Butler and others.[23] In that case, both Cl and Cl* appeared as a strong peak at 40 kcal/mol that was slightly parallel, while a much weaker contribution at 8 kcal/mol was seen in the Cl only. Based on the theoretical calculations presented here, we can ascribe the primary peak to the allowed S_2 absorption consistent with the earlier assignments. The minor peak seen at 8 kcal/mol that appears in Cl (and propargyl) likely arises from a distinct transition and gives rise to propargyl radical in the $^2B_2$ first excited state. An analogous feature is seen much more strongly in propargyl bromide dissociation suggesting perhaps that it arises from one of the triplet excitations in this region.

The repulsive dissociation dynamics observed suggest a simple model of internal energy partitioning, and we follow here the treatment of Fan and Pratt for propargyl bromide.[47] For an initially rotation-less parent molecule, the final rotational excitation of the propargyl radical must be equal in magnitude to the exit orbital angular momentum. If we assume impulsive energy release along the C-Cl bond, and direct recoil between the two fragments from this geometry, then in a classical picture we can relate the final rotational energy to the recoil energy as

$$E_{rot} = \frac{\mu_{R-Cl} b^2}{I} E_T \qquad (2)$$

where μ is the reduced mass of the propargyl-Cl system, b the exit impact parameter, and I the moment of inertia of the propargyl radical about the C axis. Using 140 pm for b based on the calculated propargyl chloride geometry, and the propargyl radical moment of inertia 8.83 $\times 10^{-46}$ kg m^2, we find $E_{rot} = 0.68 E_T$. This allows us to estimate the rotational excitation accompanying each peak, and we can attribute the balance of the available energy to vibration. The results for each identified Cl and Cl* peak are given in Table 2. The fraction of available energy appearing in vibration ranges from 13% for the fast peak to 64% for the slow peak for Cl at 236 nm, corresponding to 7 to 34 kcal/mol, respectively. Similar values are obtained for Cl*. We can obtain one estimate of the possible vibrational excitation in the propargyl radical simply by calculating the relaxation energy from the geometry of the parent molecule, which we find to be 11.7 kcal/mol. Values in Table 2 that are much higher than this suggest impulsive vibrational excitation for the direct dissociation processes, with energy randomization also possibly contributing for the predissociation near 212 nm.

5 Conclusion

DC slice imaging experiments have uncovered complex dissociation dynamics of propargyl chloride at 212 and 236 nm involving both triplet and singlet excitations. High-level theoretical calculations were used to characterize the electronic states necessary to interpret the translational energy distributions of Cl and Cl* images and their associated anisotropy. Photoexcitation to the T_1 state at 236 nm results in dissociation to ground state Cl and C_3H_3 exclusively. Photoexcitation at 236 nm also accesses T_2 and T_3, whose overlapping excitations branch to both Cl and

Cl*. The perpendicular component of the excitation is associated with the $1\,^3A''$ state, T_2, and preferably branches to Cl*, while the parallel component is associated with the $2\,^3A'$ state, T_3. Photoexcitation at 212 nm initially accesses the bound S_1 state followed by predissociation by triplet states. The repulsive dissociation dynamics likely cause impulsive vibrational excitation from direct dissociation and energy randomization in predissociation processes. Multireference ab initio calculations are essential to decipher the complex dynamics involving this high density of singlet and triplet excited electronic states.

Conflicts of interest

There are no conflicts of interest to declare.

Acknowledgments

This work was supported by the Army Research Office under award number W911NF-17-1-0099. We thank Branko Ruscic for valuable comments on the associated thermochemistry for the propargyl chloride system.

References

1 D. B. Kokh, H.-P. Liebermann and R. J. Buenker, *J. Chem. Phys.*, 2010, **132**, 074707.
2 A. Kalume, L. George, P. El-Khoury, A. N. Tarnovsky and S. Reid, *J. Phys. Chem. A*, 2010, **114**, 9919–9926.
3 G. Karras, S. Danakas and C. Kosmidis, *J. Phys. Chem. A*, 2011, **115**, 4186–4194.
4 C. P. Anderson, K. G. Spears, K. R. Wilson and R. J. Sension, *J. Chem. Phys.*, 2013, **139**, 194307.
5 A. Habartová, A. Obisesan, B. Minofar and M. Roeselová, *Theor. Chem. Acc.*, 2014, **133**, 1455.
6 A. R. Attar, A. Bhattacherjee and S. R. Leone, *J. Phys. Chem. Lett.*, 2015, **6**, 5072–5077.
7 W. G. Merrill, F. F. Crim and A. S. Case, *Phys. Chem. Chem. Phys.*, 2016, **18**, 32999–33008.
8 A. Shastri, P. J. Singh, S. Krishnakumar, A. K. Das and B. R. Sekhar, *Phys. Chem. Chem. Phys.*, 2017, **19**, 6454–6469.
9 G. Baum and J. R. Huber, *Chem. Phys. Lett.*, 1993, **203**, 261–264.
10 G. Baum and J. R. Huber, *Chem. Phys. Lett.*, 1993, **213**, 427–432.
11 G. Baum, P. Felder and J. R. Huber, *J. Chem. Phys.*, 1993, **98**, 1999–2010.
12 P. Felder and C. Demuth, *Chem. Phys. Lett.*, 1993, **208**, 21–26.
13 F. Rowland, C. Chou and P. Angelberger, *J. Phys. Chem.*, 1971, **75**, 2536–2538.
14 J. J. Lin, Y. Chen, Y. Y. Lee, Y. T. Lee and X. Yang, *Chem. Phys. Lett.*, 2002, **361**, 374–382.
15 K. Suto, Y. Sato, C. L. Reed, V. Skorokhodov, Y. Matsumi and M. Kawasaki, *J. Phys. Chem. A*, 1997, **101**, 1222–1226.
16 P. Zou, W. S. McGivern, O. Sorkhabi, A. G. Suits and S. W. North, *J. Chem. Phys.*, 2000, **113**, 7149–7157.
17 G.-J. Wang, R.-S. Zhu, H. Zhang, K.-L. Han, G.-Z. He and N.-Q. Lou, *Chem. Phys. Lett.*, 1998, **288**, 429–432.
18 Y. Liu and L. J. Butler, *J. Chem. Phys.*, 2004, **121**, 11016–11022.
19 P. Browning, D. Kitchen, M. Arendt and L. Butler, *J. Phys. Chem.*, 1996, **100**, 7765–7771.
20 M. L. Morton, L. J. Butler, T. A. Stephenson and F. Qi, *J. Chem. Phys.*, 2002, **116**, 2763–2775.
21 M. Kawasaki, K. Kasatani, H. Sato, H. Shinohara and N. Nishi, *Chem. Phys.*, 1984, **88**, 135–142.
22 Y.-R. Lee and S.-M. Lin, *J. Chem. Phys.*, 1998, **108**, 134–141.
23 L. R. McCunn, D. I. Bennett, L. J. Butler, H. Fan, F. Aguirre and S. T. Pratt, *J. Phys. Chem. A*, 2006, **110**, 843–850.
24 S. Harper, P. Calandra and S. D. Price, *Phys. Chem. Chem. Phys.*, 2001, **3**, 741–749.
25 J. C. Robinson, N. E. Sveum and D. M. Neumark, *J. Chem. Phys.*, 2003, **119**, 5311–5314.
26 H. Shen, L. Hua, Z. Cao, C. Hu and B. Zhang, *Opt. Commun.*, 2009, **282**, 387–391.
27 D. Townsend, M. P. Minitti and A. G. Suits, *Rev. Sci. Instrum.*, 2003, **74**, 2530–2539.
28 L. J. Radziemski and V. Kaufman, *J. Opt. Soc. Am.*, 1969, **59**, 424–443.
29 A. Kramida, Yu. Ralchenko, J. Reader and and NIST ASD Team, NIST Atomic Spectra Database (ver. 5.5.6), [Online]. Available: `https://physics.nist.gov/asd` [2017, April 9]. National Institute of Standards and Technology, Gaithersburg, MD., 2018.
30 J. O. F. Thompson, C. Amarasinghe, C. D. Foley and A. G. Suits, *J. Chem. Phys.*, 2017, **147**, 013913.
31 J. O. F. Thompson, C. Amarasinghe, C. D. Foley, N. Rombes, Z. Gao, S. N. Vogels, S. Y. T. van de Meerakker and A. G. Suits, *J. Chem. Phys.*, 2017, **147**, 074201.
32 T. H. Dunning Jr, *J. Chem. Phys.*, 1989, **90**, 1007–1023.
33 D. E. Woon and T. H. Dunning Jr, *J. Chem. Phys.*, 1993, **98**, 1358–1371.
34 T. H. Dunning Jr, K. A. Peterson and A. K. Wilson, *J. Chem. Phys.*, 2001, **114**, 9244–9253.
35 H.-J. Werner and P. J. Knowles, *J. Chem. Phys.*, 1985, **82**, 5053–5063.
36 P. J. Knowles and H.-J. Werner, *Chem. Phys. Lett.*, 1985, **115**, 259–267.
37 T. Shiozaki, W. Győrffy, P. Celani and H.-J. Werner, *J. Chem. Phys.*, 2011, **135**, 081106.
38 T. Shiozaki, G. Knizia and H.-J. Werner, *J. Chem. Phys.*, 2011, **134**, 034113.
39 W. Eisfeld, *J. Phys. Chem. A*, 2006, **110**, 3903–3910.
40 C. Møller and M. S. Plesset, *Phys. Rev.*, 1934, **46**, 618.
41 H.-J. Werner, P. J. Knowles, G. Knizia, F. R. Manby and M. Schütz, *WIRES Comput. Mol. Sci.*, 2012, **2**, 242–253.
42 A. Fahr, P. Hassanzadeh, B. Laszlo and R. E. Huie, *Chem. Phys.*, 1997, **215**, 59–66.
43 H. Keller-Rudek, G. K. Moortgat, R. Sander and R. Sörensen, *Earth Syst. Sci. Data*, 2013, **5**, 365.
44 J. L. Holmes and F. Lossing, *Can. J. Chem.*, 1979, **57**, 249–

252.
45 B. Ruscic, R. E. Pinzon, M. L. Morton, G. von Laszevski, S. J. Bittner, S. G. Nijsure, K. A. Amin, M. Minkoff and A. F. Wagner, *J. Phys. Chem. A*, 2004, **108**, 9979–9997.
46 A. Burcat and B. Ruscic, *Third millenium ideal gas and condensed phase thermochemical database for combustion with updates from active thermochemical tables*, Argonne National Laboratory Argonne, IL, 2005.
47 H. Fan and S. Pratt, *J. Phys. Chem. A.*, 2007, **111**, 3901–3906.
†Footnote: Electronic Supplementary Information available.